Article

BCL-XL exerts a protective role against anemia caused by radiation-induced kidney damage

Kerstin Brinkmann[1,2,*] , Paul Waring[3], Stefan P Glaser[1,2,†], Verena Wimmer[1,2], Denny L Cottle[4], Ming Shen Tham[4], Duong Nhu[1,2], Lachlan Whitehead[1,2], Alex RD Delbridge[1,2,‡], Guillaume Lessene[1,2] , Ian M Smyth[4,5] , Marco J Herold[1,2] , Gemma L Kelly[1,2], Stephanie Grabow[1,2,§,¶] & Andreas Strasser[1,2,¶,**]

Abstract

Studies of gene-targeted mice identified the roles of the different pro-survival BCL-2 proteins during embryogenesis. However, little is known about the role(s) of these proteins in adults in response to cytotoxic stresses, such as treatment with anti-cancer agents. We investigated the role of BCL-XL in adult mice using a strategy where prior bone marrow transplantation allowed for loss of BCL-XL exclusively in non-hematopoietic tissues to prevent anemia caused by BCL-XL deficiency in erythroid cells. Unexpectedly, the combination of total body γ-irradiation (TBI) and genetic loss of *Bcl-x* caused secondary anemia resulting from chronic renal failure due to apoptosis of renal tubular epithelium with secondary obstructive nephropathy. These findings identify a critical protective role of BCL-XL in the adult kidney and inform on the use of BCL-XL inhibitors in combination with DNA damage-inducing drugs for cancer therapy. Encouragingly, the combination of DNA damage-inducing anti-cancer therapy plus a BCL-XL inhibitor could be tolerated in mice, at least when applied sequentially.

Introduction

Evasion of apoptotic cell death is a hallmark of cancer (Hanahan & Weinberg, 2000, 2011), and direct activation of the cell death machinery by BH3-mimetic drugs represents an attractive therapeutic strategy (Merino *et al*, 2018). Apoptosis is controlled by pro- and anti-apoptotic members of the BCL-2 protein family (Tait & Green, 2010), with the transcriptional or post-transcriptional activation of the pro-apoptotic BH3-only members of the BCL-2 family (e.g., BIM, PUMA) being its initiator. The BH3-only proteins bind with high affinity to the anti-apoptotic BCL-2 family members (e.g., BCL-2, BCL-XL), thereby unleashing the pro-apoptotic effector proteins BAX and BAK to cause mitochondrial outer membrane permeabilization (MOMP). MOMP causes the release of activators of the caspase cascade that causes cell demolition (Riedl & Salvesen, 2007; Tait & Green, 2010). The extent of MOMP and apoptosis is considered key determinants of therapeutic success of anti-cancer therapeutics (Del Gaizo Moore & Letai, 2013). BH3-only proteins, particularly PUMA (Villunger *et al*, 2003) and BIM (Bouillet *et al*, 1999a), are critical for the killing of malignant (and non-transformed) cells by diverse anti-cancer agents. As a consequence of genetic or epigenetic changes, many cancers show a reduction in pro-apoptotic BH3-only proteins or overexpression of pro-survival BCL-2 proteins (Uhlen *et al*, 2005; Beroukhim *et al*, 2010; Uhlen *et al*, 2017). Certain cancer cells can be killed by the loss or inhibition of a single pro-survival BCL-2 family member (Glaser *et al*, 2012; Kelly *et al*, 2014), whereas others require loss/inhibition of two or more of these proteins (Campbell & Tait, 2018). Several small-molecule inhibitors of pro-survival BCL-2 proteins (BH3-mimetic drugs) have been developed (Adams & Cory, 2018). Even though BH3-mimetics can potently kill diverse cancer cells *in vitro* and *in vivo*, the safe clinical use of some of these drugs remains challenging due to the obligate roles of pro-survival BCL-2 proteins for the survival of normal cells in healthy tissues (Adams & Cory, 2018).

1 The Walter and Eliza Hall Institute of Medical Research, Melbourne, Vic., Australia
2 Department of Medical Biology, University of Melbourne, Melbourne, Vic., Australia
3 Department of Surgery, University of Melbourne, Melbourne, Vic., Australia
4 Department of Anatomy and Developmental Biology, Development and Stem Cell Program Monash Biomedicine Discovery Institute (BDI), Monash University, Melbourne, Vic., Australia
5 Department of Biochemistry and Molecular Biology, Monash University, Melbourne, Vic., Australia
 *Corresponding author. Tel: +61 3 9345 2555; E-mail: brinkmann.k@wehi.edu.au
 **Corresponding author. Tel: +61 3 9345 2555; E-mail: strasser@wehi.edu.au
 ¶These authors are contributed equally to this work as senior authors
 †Present address: Boehringer Ingelheim RCV GmbH & Co KG, Vienna, Austria
 ‡Present address: Putnam Associates, Boston, MA, USA
 §Present address: Blueprint Medicines, Cambridge, MA, USA

Gene deletion studies in mice have helped identify the critical roles of the different pro-survival BCL-2 family members. Loss of A1/BFL-1 causes minor reductions in certain hematopoietic cell subsets (Schenk *et al*, 2017; Tuzlak *et al*, 2017), and loss of BCL-W causes male sterility (Print *et al*, 1998). BCL-2-deficient mice die soon after weaning due to polycystic kidney disease and also present with reductions in mature B and T lymphocytes and melanocytes (causing premature graying) (Veis *et al*, 1993). These abnormalities could be prevented by concomitant loss of pro-apoptotic BIM (Bouillet *et al*, 2001). Constitutive loss of MCL-1 causes embryonic lethality prior to implantation (E3.5) (Rinkenberger *et al*, 2000), and tissue-restricted deletion revealed that many cell types, including cardiomyocytes (Thomas *et al*, 2013; Wang *et al*, 2013), neurons (Arbour *et al*, 2008), and several hematopoietic cell subsets (Opferman *et al*, 2005) require MCL-1 for survival. Loss of *Bcl-x* causes embryonic lethality at ~ E13.5 with aberrant death of neurons and immature hematopoietic cells (Motoyama *et al*, 1995). Conditional deletion of *Bcl-x* only in erythroid cells causes fatal anemia (Wagner *et al*, 2000), and loss of just one allele of *Bcl-x* impairs male fertility (Rucker *et al*, 2000) and reduces platelet numbers (Mason *et al*, 2007).

BH3-mimetic drugs that selectively target BCL-XL (A1331852) (Lessene *et al*, 2013) or BCL-2 (ABT-199/venetoclax) (Souers *et al*, 2013) or compounds that inhibit BCL-XL, BCL-2, and BCL-W (ABT-737, ABT-263) (Oltersdorf *et al*, 2005; Tse *et al*, 2008) have been developed. Even though inhibitors of BCL-XL can efficiently kill diverse cancer cells, by themselves or in combination with additional anti-cancer agents (Oltersdorf *et al*, 2005; Cragg *et al*, 2007; Cragg *et al*, 2008; Tse *et al*, 2008), these compounds are progressing slowly in the clinic. This is in part due to the fact that the essential roles of BCL-XL in the adult (beyond its role in hematopoietic cells) are not clearly understood. Here we investigated the impact of inducible loss of BCL-XL in adult mice. This revealed that BCL-XL loss is tolerated throughout the body as long as the hematopoietic cells remain BCL-XL-sufficient. However, mice that had been γ-irradiated (for bone marrow transplantation) and then subjected to loss of BCL-XL developed secondary anemia due to chronic renal failure with secondary obstructive nephropathy

characterized by renal tubular epithelial cell apoptosis. This morbidity could be markedly delayed, although not abrogated, by the concomitant loss of pro-apoptotic PUMA or BIM. These findings predict potential toxicities and their underlying mechanisms resulting from combinations of BCL-XL inhibitors with DNA damage-inducing anti-cancer therapeutics.

Results

Impact of induced deletion of BCL-XL in adult mice

Bcl-x$^{-/-}$ embryos die ~ E13.5 due to loss of neuronal and erythroid cells (Motoyama *et al*, 1995). Mice with hypomorphic mutations in the *Bcl-x* gene are viable but develop severe thrombocytopenia and anemia (Mason *et al*, 2007). We wanted to explore the consequences of inducible loss of BCL-XL in adult mice. For this, we crossed *Bcl-x*$^{fl/fl}$ mice with *RosaCreERT2* mice that express a CreERT2 fusion protein in all tissues. CreERT2 is normally kept inactive in the cytoplasm by binding to HSP90 but can be activated by tamoxifen (Vooijs *et al*, 2001). Even though BCL-XL is essential for neuronal cell survival (Motoyama *et al*, 1995), we did not expect any neuronal abnormalities upon tamoxifen treatment in *Bcl-x*$^{fl/fl}$; *RosaCreERT2*$^{+/Ki}$ mice since tamoxifen administered by oral gavage did not efficiently drive CreERT2-mediated deletion of the *Bcl-x*-floxed genes in the brain, as shown by Southern blotting (Appendix Fig S1A). Almost complete deletion of the *Bcl-x* gene was achieved in most other tissues, including the spleen, kidney, liver, pancreas, intestine, and lung, whereas deletion in the testis was ~ 70%.

As reported (Motoyama *et al*, 1995; Wagner *et al*, 2000), we found that induced loss of BCL-XL in adult mice caused fatal thrombocytopenia and anemia with a median survival of ~ 25 days (Fig 1A). Accordingly, the BCL-XL-deleted mice presented with significant decreases in platelets, red blood cells (RBCs), hemoglobin content (HGB), and hematocrit (HCT) (Fig 1C–F), accompanied by massively enlarged spleens due to compensatory erythropoiesis in this tissue (Fig 1G–I).

Figure 1. The inducible deletion of BCL-XL causes severe anemia even in chimeric mice that are BCL-XL sufficient in all hematopoietic cell populations.

A   *Bcl-x*$^{fl/fl}$;*RosaCreERT2*$^{+/Ki}$ (*n* = 12) or, as controls, *Bcl-x*$^{fl/fl}$ (*n* = 6), and *RosaCreERT2*$^{+/Ki}$ (*n* = 16) mice (age 9–12 weeks, males and females) were treated with tamoxifen (200 mg/kg body weight administered in 3 daily doses by oral gavage) to induce CreERT2-mediated deletion of the floxed *Bcl-x* alleles. Mice were monitored for up to 200 days post-treatment with tamoxifen. Data are presented as % survival post-treatment with tamoxifen, and statistical significance was assessed using the Mantel–Cox (log-rank) test; ****P < 0.0001.

B   *Bcl-x*$^{fl/fl}$;*RosaCreERT2*$^{+/Ki}$ (*n* = 24) or, as controls, *Bcl-x*$^{fl/fl}$ (*n* = 9), and *RosaCreERT2*$^{+/Ki}$ (*n* = 6) mice (males and females, aged 8–14 weeks, numbers also indicated in the figure) were lethally γ-irradiated (2 × 5.5 Gy, 3 h apart) and reconstituted with bone marrow from UBC-GFP mice (referred to as GFP-Chimeras). After 8 weeks, reconstituted mice were treated with tamoxifen (200 mg/kg body weight administered in 3 daily doses oral gavage) and monitored for up to 200 days (termination of the experiment). Data are presented as % survival post-treatment with tamoxifen, and statistical significance was assessed using the Mantel–Cox (log-rank) test; ****P < 0.0001.

C–F   Total counts of (C) platelets, (D) red blood cells (RBC), (E) hemoglobin (HGB) content, and (F) hematocrit (HCT) of tamoxifen-treated *Bcl-x*$^{fl/fl}$;*RosaCreERT2*$^{+/Ki}$ (*n* = 8) or, as controls, *Bcl-x*$^{fl/fl}$ (*n* = 6) and *RosaCreERT2*$^{+/Ki}$ (*n* = 12) and *Bcl-x*$^{fl/fl}$;*RosaCreERT2*$^{+/Ki}$;*GFP-Chimera* (*n* = 21) or, as controls, *Bcl-x*$^{fl/fl}$;*GFP-Chimera* (*n* = 6) and *RosaCreERT2*$^{+/Ki}$;*GFP-Chimera* (*n* = 6) mice were determined by ADVIA. Data are presented as mean ± SEM. Each data point represents an individual mouse. Statistical significance was assessed using Student's *t*-test; ****P < 0.0001.

G   Spleen weights were measured in sick mice (at sacrifice) or, for the healthy control mice, at the termination of the experiment. Data are presented as mean ± SEM. Each data point represents an individual mouse and numbers are indicated. Statistical significance was assessed using Student's *t*-test; ****P < 0.0001.

H   Representative image of enlarged spleens from two *Bcl-x*$^{fl/fl}$;*RosaCreERT2*$^{Ki/+}$ mice and age-matched control *Bcl-x*$^{fl/fl}$ and *RosaCreERT2*$^{+/Ki}$ mice (34 days after treatment).

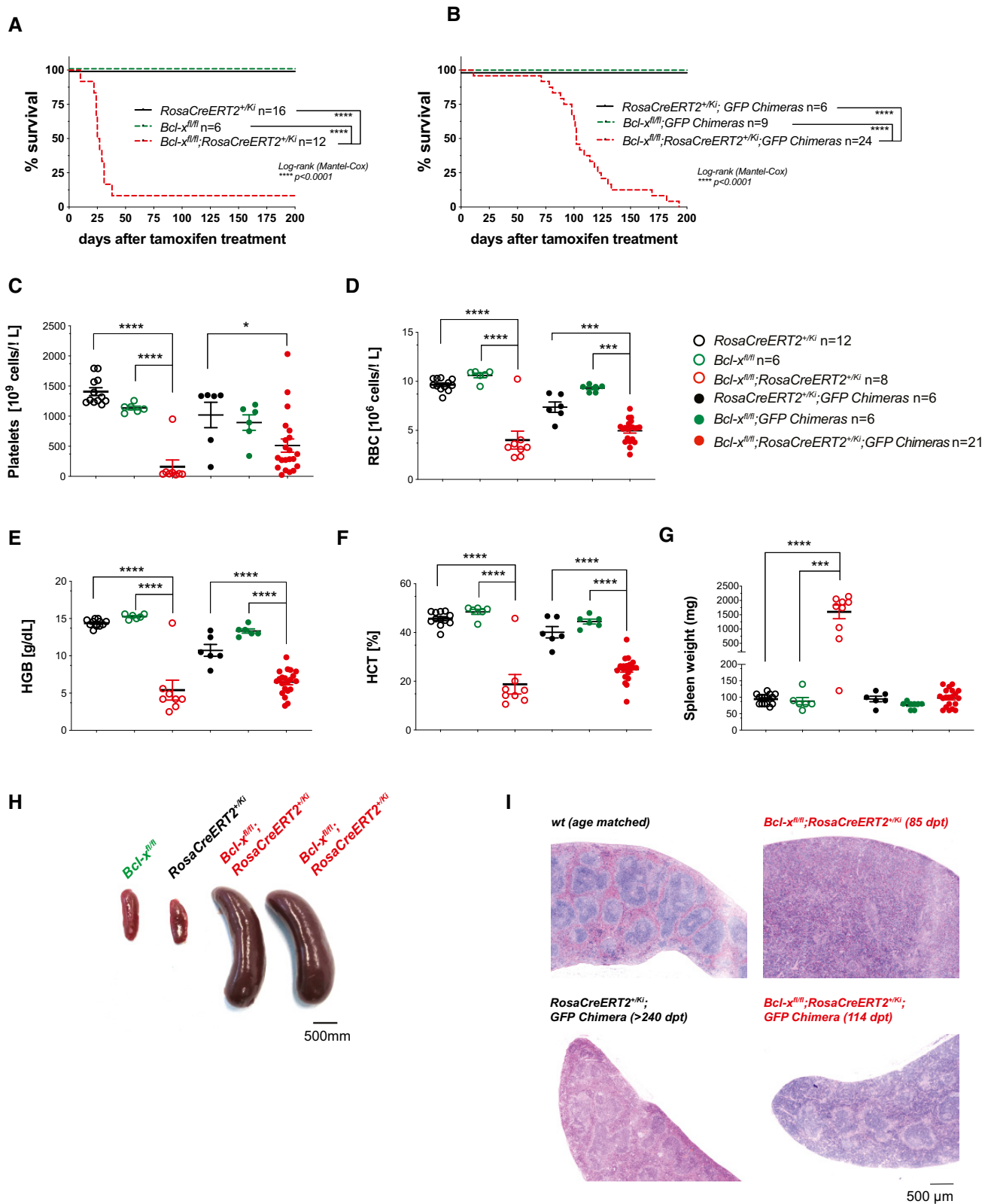I   Histological analysis of H&E-stained sections of spleens of tamoxifen-treated mice of the indicated genotypes.

Figure 1.

To identify the essential functions of BCL-XL in non-hematopoietic tissues of adult mice, we generated bone marrow chimeras: *Bcl-x^{fl/fl};RosaCreERT2^{+/Ki}* mice that had been lethally irradiated and reconstituted with bone marrow cells from UBC-GFP mice (GFP-Chimeras; experimental design in Appendix Fig S1B). Unexpectedly, these chimeric animals also presented with severe anemia and

thrombocytopenia after loss of BCL-XL, albeit at a considerably later time (Fig 1C–F). Around day 100 post-treatment with tamoxifen, the *Bcl-x^{fl/fl};RosaCreERT2^{+/Ki};GFP-Chimeras* appeared runty, lethargic, and anemic and had to be sacrificed according to our animal ethics guidelines after > 15% body weight loss (median survival = 102 days, Fig 1B). Notably, sick *Bcl-x^{fl/fl};Rosa-CreERT2^{+/Ki};GFP-Chimeras* did not present with splenomegaly (Fig 1G) or an increase in the red pulp area of the spleen (Fig 1I), which are hallmarks of primary anemia caused by loss of BCL-XL in erythroid and megakaryocytic cell populations (Fig 1G–I). Importantly, the tamoxifen-treated *Bcl-x^{fl/fl};GFP-Chimera* and *Rosa-CreERT2^{+/Ki};GFP-Chimera* control mice all survived without any adverse events for > 240 days (termination of the experiment).

These findings demonstrate that inducible loss of BCL-XL in all tissues of adult mice (including hematopoietic cells) causes primary anemia and thrombocytopenia, whereas the combination of total body γ-irradiation (TBI), followed by rescue with a UBC-GFP hematopoietic system, and inducible loss of BCL-XL only in non-hematopoietic cells causes secondary anemia.

The secondary anemia in mice caused by the combination of γ-radiation and inducible deletion of BCL-XL is not driven by inflammation, hematopoietic malignancy, or liver damage

TBI is commonly used for the treatment of hematologic malignancies, often alongside high dose chemotherapy, prior to hematopoietic stem/progenitor cell (HSPC) transplantation. TBI causes many side-effects, including nausea, diarrhea, sensitive skin, and hair loss, that are temporary. However, TBI can also cause severe long-term damage to several organs, such as the lung, trachea, and mouth (radiation-induced pneumonitis, fibrosis, oral mucositis) (Marks *et al*, 2003; Mehta, 2005), reproductive system (radiation-induced infertility) (Ogilvy-Stuart & Shalet, 1993), liver (radiation-induced liver disease) (Kim & Jung, 2017), gastrointestinal tract (radiation-induced gastric mucositis, radiation-induced gastrointestinal syndrome) (Francois *et al*, 2013; Olcina & Giaccia, 2016), or kidney (radiation-induced nephropathy) (Cohen, 2000; Cohen & Robbins, 2003). Furthermore, TBI can also initiate secondary malignancies (Dracham *et al*, 2018).

The above-mentioned TBI-induced pathologies frequently cause secondary anemia (Weiss & Goodnough, 2005; Davis & Littlewood, 2012). For example, hematologic malignancies impair the production of RBCs in the bone marrow as a consequence of competing for essential growth factors, the production of reactive oxygen species (ROS) and pro-inflammatory cytokines that damage erythroid progenitors (Weiss & Goodnough, 2005; Davis & Littlewood, 2012). Moreover, a robust inflammatory response is observed upon radiation-induced damage to the gastrointestinal tract (Olcina & Giaccia, 2016). Pro-inflammatory cytokines (e.g., IL-6, TNF-α) interfere with the production of erythropoietin (EPO) and the availability of iron, both crucial for RBC development. Furthermore, inflammatory cytokines enhance the production of white blood cells (WBCs) and can thereby decrease the differentiation of progenitors into RBCs (Weiss & Goodnough, 2005). We did not detect signs of ongoing inflammation in the tamoxifen-treated *Bcl-x^{fl/fl};RosaCreERT2^{+/Ki}; GFP-Chimeras* as shown by the observation that the numbers of WBCs (Fig 2A), including lymphocytes, neutrophils, basophils, eosinophils, and monocytes, were all within the normal range (Appendix Fig S2A). The neutrophil-to-lymphocyte ratio (NLR), even though increased in the tamoxifen-treated *Bcl-x^{fl/fl};Rosa-CreERT2^{+/Ki};GFP-Chimeras,* was still within the normal range (Fig 2B). Moreover, no signs of hematologic malignancies, such as increased numbers of leukocytes, were observed in the blood or bone marrow of the tamoxifen-treated *Bcl-x^{fl/fl};RosaCreERT2^{+/Ki}; GFP-Chimeras* (Fig 2A and C).

The liver represents the primary storage site of iron and source of hepcidin that are both essential for RBC production. Hence, secondary anemia can result from liver damage. Histological analysis failed to reveal any abnormalities in the livers of the tamoxifen-treated *Bcl-x^{fl/fl};RosaCreERT2^{+/Ki};GFP-Chimeras* (Fig 2D), and no marked increases in the liver enzyme ALT or unconjugated bilirubin were detected in their sera (Fig 2E). However, these animals presented with increased levels of AST (Fig 2E), but unlike ALT, AST is also found in the heart, skeletal muscle, kidney, and RBCs. Thus, with the lack of other indicators of liver pathology, we attributed this AST increase to non-liver toxicity.

These findings demonstrate that the secondary anemia in the tamoxifen-treated *Bcl-x^{fl/fl};RosaCreERT2^{+/Ki};GFP-Chimeras* is not a consequence of erythroid cell destruction, hematologic malignancy, chronic infection, inflammation, nor liver damage. Instead, these results suggest that the secondary anemia might be caused by radiation-induced kidney damage.

Figure 2. The combination of γ-radiation and inducible deletion of BCL-XL causes neither inflammation, hematopoietic malignancy, nor liver damage.

Bcl-x^{fl/fl};RosaCreERT2^{+/Ki} (*n* = 8) or, as controls, *Bcl-x^{fl/fl}* (*n* = 6), and *RosaCreERT2^{+/Ki}* (*n* = 12) mice as well as *Bcl-x^{fl/fl};RosaCreERT2^{+/Ki}; GFP-Chimeras* (*n* = 21), or as controls, *Bcl-x^{fl/fl};GFP-Chimeras* (*n* = 6), and *RosaCreERT2^{+/Ki};GFP-Chimeras* (*n* = 6) (age 8–14 weeks, males and females) were treated with tamoxifen (200 mg/kg body weight administered in 3 daily doses by oral gavage) to induce CreERT2-mediated deletion of the floxed *Bcl-x* alleles.

A   Total white blood cell counts (WBC) were analyzed by ADVIA in sick mice or at the termination of the experiment (healthy control mice). Data are presented as mean ± SEM. Each data point represents an individual mouse and *n* numbers are indicated above. Statistical significance was assessed using Student's t-test. No statistically significant differences were observed.

B   The neutrophil/lymphocyte ratio (NLR) is presented as mean ± SEM for sick *Bcl-x^{fl/fl};RosaCreERT2^{+/Ki};GFP-Chimeras* (*n* = 21) or healthy control *RosaCreERT2^{+/Ki};GFP-Chimeras* (*n* = 6) at the termination of the experiment. Data are presented as mean ± SEM. Each data point represents an individual mouse. Statistical significance was assessed using Student's t-test; *P < 0.05.

C   Histological analysis of H&E-stained sections of the sternum of sick *Bcl-x^{fl/fl};RosaCreERT2^{+/Ki};GFP-Chimeras* or healthy wild-type and *RosaCreERT2^{+/Ki};GFP-Chimera* control mice at the indicated time points post-treatment with tamoxifen (dpt = days post-treatment).

D   Histological analysis of H&E-stained sections of the livers of sick mice or age-matched healthy control wild-type mice or healthy *RosaCreERT2^{+/Ki};GFP-Chimeras* at the termination of the experiment (dpt = days post-treatment).

E   ALT (left panel), AST (middle panel), and bilirubin levels (right panel) in the serum were determined in sick *Bcl-x^{fl/fl};RosaCreERT2^{+/Ki};GFP-Chimeras* (*n* = 18) or in healthy *RosaCreERT2^{+/Ki};GFP-Chimeras* (*n* = 4) at the termination of the experiment. Data are presented as mean ± SEM. Each data point represents one individual mouse. Statistical significance was assessed using Student's t-test; **P < 0.01. nd = not detected.
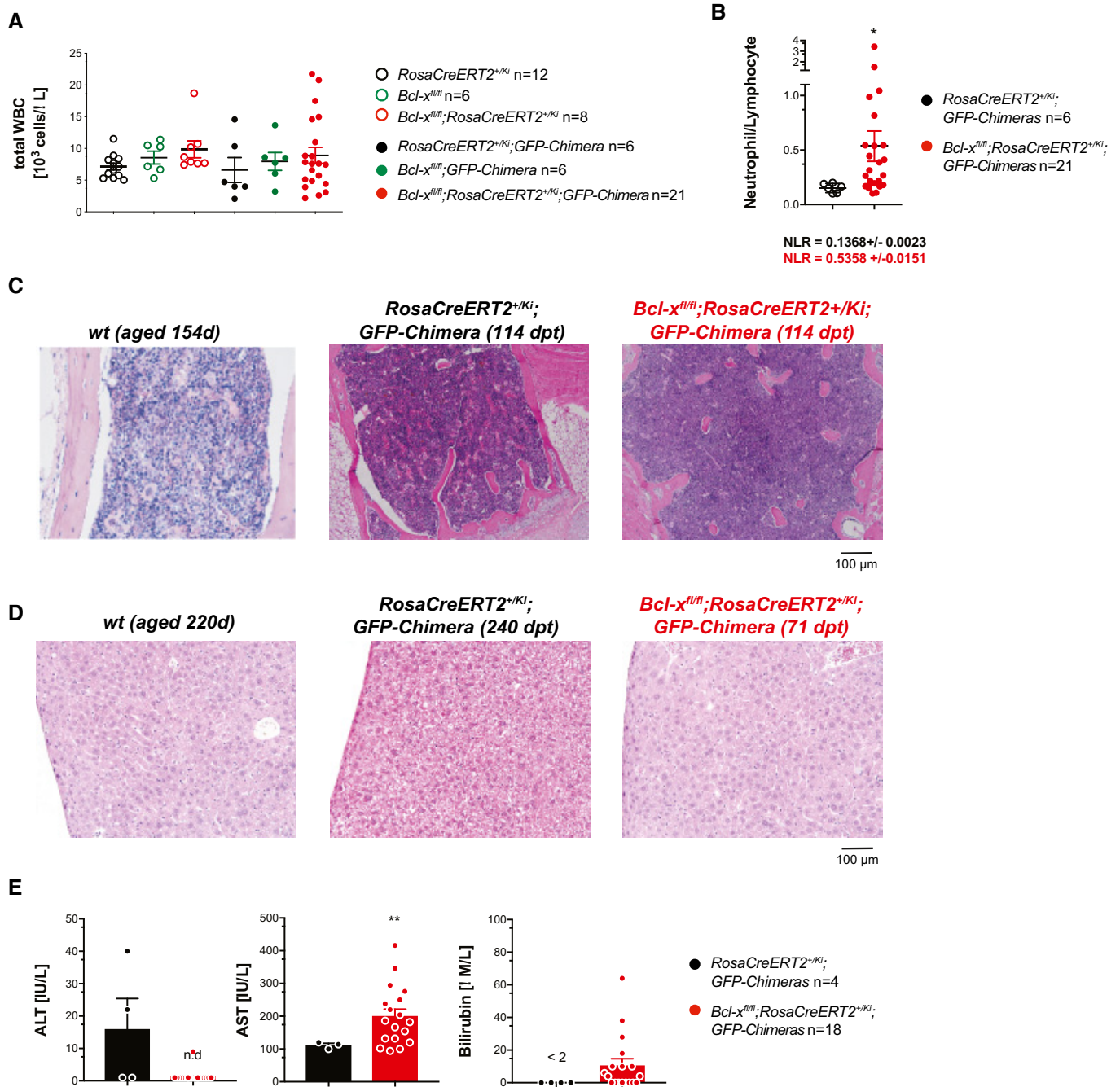
Figure 2.

The combination of γ-radiation and inducible deletion of BCL-XL causes severe kidney damage in adult mice

EPO stimulates erythropoiesis and is produced in response to cellular hypoxia in the kidney by interstitial fibroblasts adjacent to the renal proximal convoluted tubule and peritubular capillaries. Acute and chronic kidney disease that damages these cells decreases the production of EPO, thereby compromising the generation of erythroid progenitors (CFU-e) and thus RBC production. We hypothesized that the secondary anemia observed in tamoxifen-treated *Bcl-x^{fl/fl};RosaCreERT2^{+/Ki};GFP-Chimeras* results from damage to the EPO-secreting

cells in the kidney. Accordingly, urine tests showed severe proteinuria in sick tamoxifen-treated *Bcl-x^{fl/fl};RosaCreERT2^{+/Ki};GFP-Chimeras* (Appendix Fig S3A), and due to increased urination, the bedding of their cages had to be changed frequently.

The kidneys of these sick mice were abnormally small and yellow (Fig 3A and B). Histological analysis revealed severe renal tubulointerstitial disease with segmental areas showing diminution of the renal tubules, interstitial fibrosis, and patchy chronic inflammation with focal and segmental glomerular changes and thickening of renal arterioles. The renal medulla and papillae contained intraluminal calcified cellular debris and crystalline

Figure 3.

precipitates within the collecting ducts and dilated loops of Henle, where urine is concentrated (Fig 3C). This was sometimes accompanied by intraluminal multi-nucleated macrophages, reminiscent of the changes seen in myeloma nephropathy. The glomeruli in the affected segments showed secondary focal and segmental sclerosis. These structural changes were additionally visualized using confocal microscopy (Appendix Fig S4).

The kidney damage was confirmed using multi-photon microscopy (Fig 3D). To avoid spurious signals due to non-specific antibody binding, the kidneys were visualized using short wavelength auto-fluorescence (blue) and second harmony generation (SHG) (green). Materials that efficiently generate SHG include type-1-collagen, myosin, tubulin, or non-linear crystals and minerals. The intensity of short wavelength auto-fluorescence provides information on the metabolic activity as it visualizes metabolic cofactors, including NADH and NADPH. Accordingly, higher short wavelength auto-fluorescence was observed in the mitochondria-rich proximal tubular cells compared to the distal tubular cells in the kidneys from healthy control mice. In contrast, a significant reduction in metabolically active cells was observed in the atrophic segmental areas in the kidneys from sick tamoxifen-treated *Bcl-x^{fl/fl};RosaCreERT2^{+/Ki};GFP-Chimeras* (Fig 3D). The above-mentioned precipitates within the dilated loops of Henle generated a strong SHG signal, confirming their crystalline nature (Fig 3D).

These findings demonstrate that the combination of TBI and *Bcl-x*-deletion causes fatal renal tubulointerstitial disease.

The combination of γ-radiation and inducible deletion of BCL-XL causes apoptosis of tubular epithelial cells in the kidney

Loss or inhibition of pro-survival BCL-XL causes apoptotic cell death (Adams & Cory, 2007). We therefore performed TUNEL staining that detects 3′-hydroxyl termini in double-strand DNA breaks, a hallmark of apoptotic cells (Gavrieli *et al*, 1992; Gorczyca *et al*, 1992), to determine whether inducible loss of BCL-XL, TBI, or their combination caused apoptosis in renal cells. We observed significantly increased numbers of TUNEL⁺ cells in kidney sections from sick tamoxifen-treated *Bcl-x^{fl/fl};RosaCreERT2^{+/Ki};GFP-Chimeras*. The TUNEL⁺ cells were mainly localized in the proximal tubular epithelium within segments showing tubulointerstitial disease. In contrast, only occasional apoptotic cells were found in sections from healthy control animals (Fig 4A and B).

Notably, 24 h following tamoxifen treatment (8 weeks post-TBI), TUNEL⁺ cells were detected in *Bcl-x^{fl/fl};RosaCreERT2^{+/Ki};*

GFP-Chimeras and in control *RosaCreERT2^{+/Ki};GFP-Chimeras*, *Bcl-x^{fl/fl};RosaCreERT2^{+/Ki}* mice and *RosaCreERT2^{+/Ki}* mice (Fig 4A and B). This indicates that both TBI and loss of BCL-XL by themselves induce renal proximal tubular epithelial cell apoptosis. However, in contrast to the control mice that were able to recover from TBI-induced kidney damage, the additional loss of BCL-XL resulted in more extensive apoptosis in the renal tubular epithelium with their cellular debris accumulating in the renal loops of Henle and collecting ducts. This caused secondary obstruction, glomerulopathy, and interstitial nephropathy with damage to the adjacent EPO-secreting peritubular interstitial cells.

These findings demonstrate that the combination of TBI and inducible loss of BCL-XL causes extensive apoptosis in the renal proximal convoluted tubular epithelium, leading to chronic renal failure and secondary anemia.

Concomitant loss of BIM or PUMA delays kidney disease with secondary anemia caused by radiation and the induced loss of BCL-XL in adult mice

We next investigated which BH3-only protein was critical for apoptosis in the renal tubular epithelium in tamoxifen-treated *Bcl-x^{fl/fl};RosaCreERT2^{+/Ki};GFP-Chimeras*. We focused on BIM and PUMA because both play critical roles in DNA damage-induced apoptosis in diverse cell types (Bouillet *et al*, 1999a; Villunger *et al*, 2003; Erlacher *et al*, 2005). Notably, TBI of wild-type mice resulted in increased expression of the DNA damage responsive genes *Puma* and *Bax* in isolated proximal tubular epithelium cells (Appendix Fig S5) suggesting that TBI sensitizes proximal tubular epithelium cells toward the later loss of BCL-XL by changing the expression pattern of pro-apoptotic members of the BCL-2 family. Moreover, we found a consistent decrease in the expression of anti-apoptotic BCL-2 family members, such as *Bcl-2* and *A1*, and increases in pro-apoptotic family members, such as *Puma* and *Bim*, in the *Bcl-xl^{fl/fl};RosaCreERT2^{+/Ki}*-GFP-Chimeras when compared to *RosaCreERT2^{+/Ki}* control mice. The levels of the executioners of the intrinsic apoptotic pathway, BAX and BAK, were not markedly altered (Appendix Fig S5).

In line with these observations, we observed a significant extension of survival of tamoxifen-treated *Bcl-x^{fl/fl};RosaCreERT2^{+/Ki};Bim^{+/−};GFP-Chimeras* (median survival 159 days; *P* < 0.0001), *Bcl-x^{fl/fl};RosaCreERT2^{+/Ki};Bim^{−/−};GFP-Chimeras* (221 days; *P* < 0.0001), *Bcl-x^{fl/fl};RosaCreERT2^{+/Ki};Puma^{+/−};GFP-Chimeras* (125 days) *Bcl-x^{fl/fl};RosaCreERT2^{+/Ki};Puma^{−/−};GFP-Chimeras* (281 days; *P* < 0.0001) compared to the *Bcl-x^{fl/fl};RosaCreERT2^{+/Ki};GFP-Chimeras* (102 days)

A

B
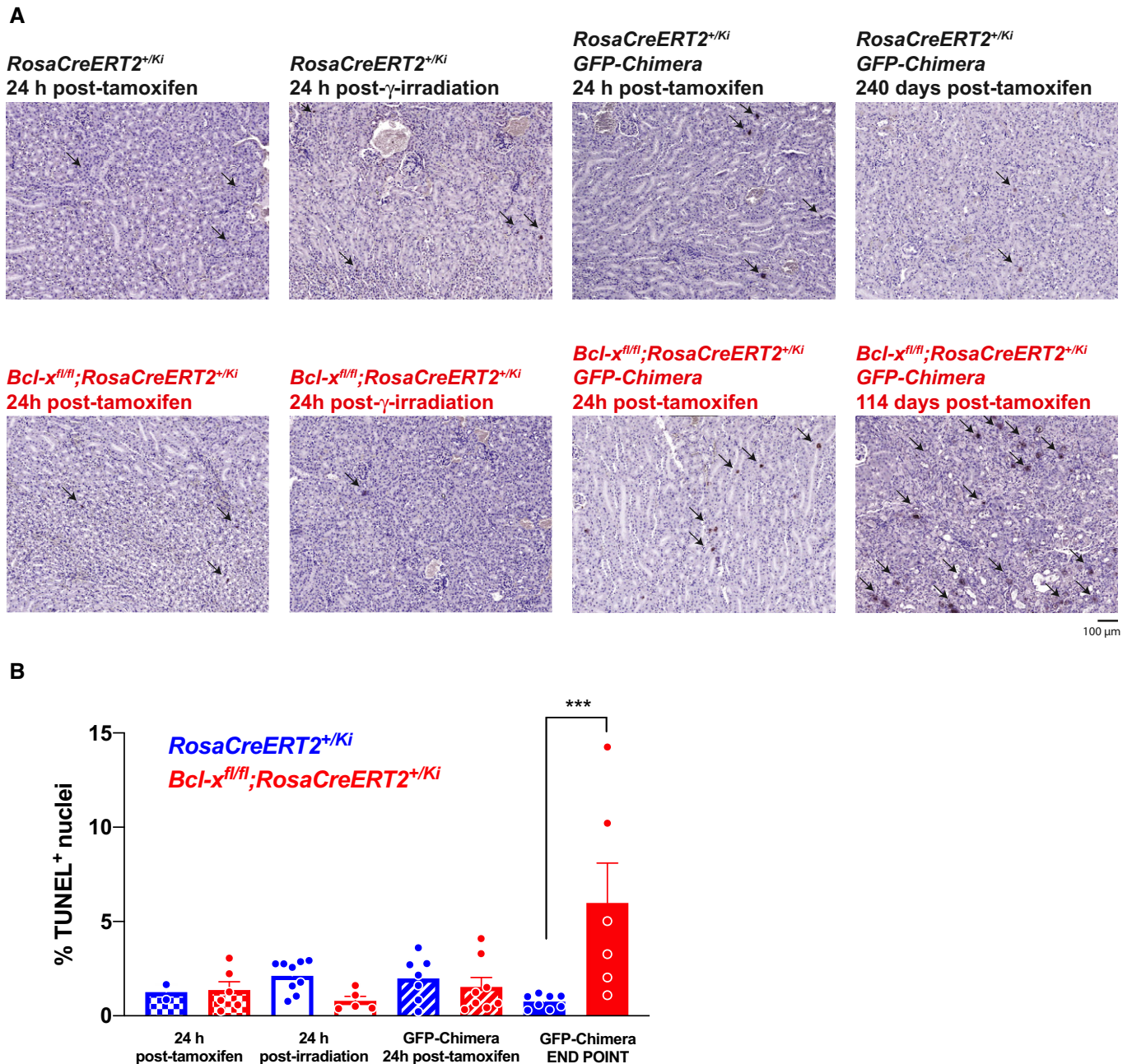
Figure 4. The combination of γ-radiation and inducible deletion of BCL-XL causes apoptosis of proximal renal tubule epithelial cells.

A TUNEL staining of kidney sections from control *RosaCreERT2*[+/Ki], *Bcl-x*^{fl/fl}*;RosaCreERT2*[+/Ki], *RosaCreERT2*[+/Ki]*;GFP-Chimeras*, or *Bcl-x*^{fl/fl}*;RosaCreERT2*[+/Ki]*;GFP-Chimeras* at the indicated time points post-tamoxifen treatment (200 mg/kg/body weight administered in 3 daily doses by oral gavage) or γ-irradiation (2 × 550 Rad), as indicated. Slides were counterstained with hematoxylin. Arrow heads indicate examples of TUNEL[+] (apoptotic) cells.

B TUNEL^{+} cells were quantified using a personalized script for the Image J software. Kidney sections were divided into ~ 40 microscopic images, and the total numbers of blue and brown (TUNEL[+]) nuclei were determined. The percentages of TUNEL[+] nuclei were calculated for each picture. The average value for each kidney section was then determined and plotted as a single data point. Error bars represent SEM from at least 3 independent samples for each genotype and treatment. Statistical significance was assessed using one-way ANOVA analysis with Tukey's multiple comparisons test (comparing control *RosaCreERT2*[+/Ki] (24 h post-tamoxifen $n = 2$, 24 h post-γ-irradiation $n = 9$) with *Bcl-x*^{fl/fl}*;RosaCreERT2*[+/Ki] (24 h post-tamoxifen $n = 6$, 24 h post-γ-irradiation $n = 5$) and control *RosaCreERT2*[+/Ki]*;GFP-Chimeras* (24 h post-tamoxifen $n = 7$, End point $n = 8$) with *Bcl-x*^{fl/fl}*;RosaCreERT2*[+/Ki]*;GFP-Chimeras* (24 h post-tamoxifen $n = 8$, End point $n = 6$) (***$P < 0.001$).

(Fig 5A and B). Combined loss of one allele of *Bim* plus one allele of *Puma* (*Bcl-x*^{fl/fl}*;RosaCreERT2*[+/Ki]*;Bim*^{+/−}*;Puma*^{+/−}*;GFP-Chimeras*) resulted in a similar extension of lifespan as seen for mice lacking either both alleles of *Bim* or both alleles of *Puma* (median survival 243 days; $P < 0.0001$) (Fig 5A and B). Nevertheless, all these mice ultimately presented with similar pathology as the tamoxifen-treated
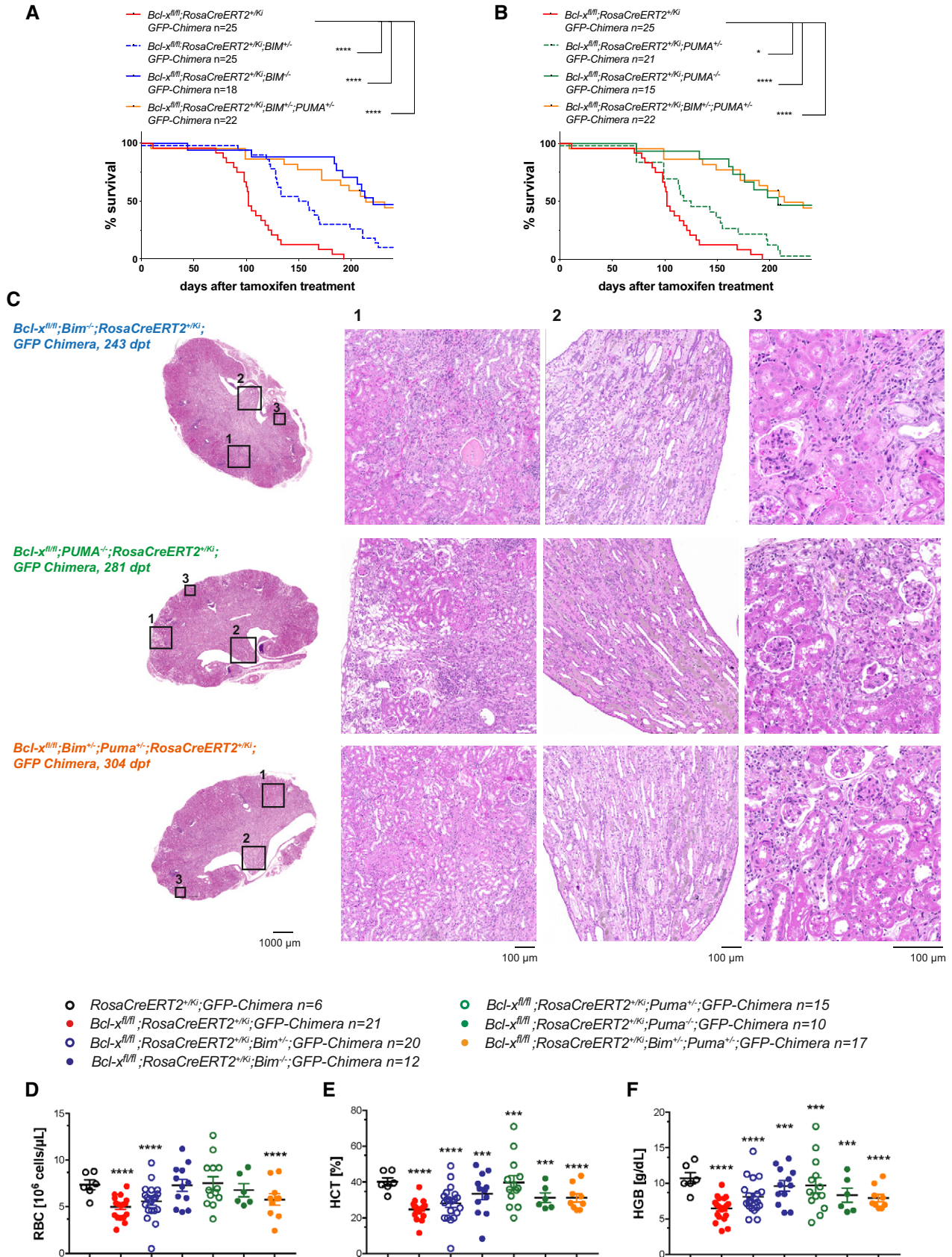
Figure 5.

$Bcl-x^{fl/fl}$;$RosaCreERT2^{+/Ki}$;GFP-$Chimeras$, including kidney damage (Fig 5C) and secondary anemia (Fig 5D–F).

These results demonstrate that BIM and PUMA play critical overlapping roles in the induction of apoptosis of renal tubular epithelial cells caused by the combination of TBI and inducible loss of BCL-XL.

Pharmacological inhibition of BCL-XL in combination with DNA-damaging anti-cancer therapeutics does not cause kidney disease with secondary anemia

BH3 mimetic drugs targeting select anti-apoptotic BCL-2 family members represent promising novel agents in cancer therapy (Merino *et al*, 2018). The BCL-XL-specific inhibitor A1331852 (Lessene *et al*, 2013) has not yet entered clinical trials, mostly due to its on-target toxicity in platelets that is also seen with ABT-263/navitoclax that inhibits BCL-XL, BCL-2, and BCL-W (Mason *et al*, 2007; Wilson *et al*, 2010; Leverson *et al*, 2015). Nevertheless, many cancers depend on BCL-XL for sustained growth (Campbell & Tait, 2018; Merino *et al*, 2018) and extensive work is being conducted to develop modes of administration and dose schedules for the safe use of BCL-XL inhibitors (Khan *et al*, 2019). Our present

data indicate that the combination of BCL-XL inhibitors with DNA damage-inducing therapies might cause renal toxicity with secondary anemia. However, drug-mediated inhibition of a pro-survival BCL-2 family member often exerts considerably less severe impact than genetic loss of this protein, as demonstrated for MCL-1 (Kotschy *et al*, 2016). Thus, in contrast to the genetic deletion of *Bcl-x* resulting in a permanent loss of BCL-XL protein, the pharmacological inhibition of BCL-XL for a defined period might be tolerated, even in combination with DNA damage-inducing chemotherapeutics. To test this hypothesis, we treated wild-type mice that had been γ-irradiated and reconstituted with UBC-GFP bone marrow with a clinically relevant and well-tolerated dose of the BCL-XL inhibitor A1331852, for which a clear PK/PD effect has been reported (Leverson *et al*, 2015; Le Wang *et al*, 2020). Additionally, we treated wild-type mice with a combination of clinically relevant doses of either of the DNA-damaging drugs 5-fluorouracil (5-FU) or cyclophosphamide plus A1331852. No adverse effects of any of these combination treatments were detected for at least 150 days (Fig 6A and B). As expected (Mason *et al*, 2007; Wilson *et al*, 2010; Leverson *et al*, 2015; Merino *et al*, 2018), the administration of A1331852 resulted in on-target platelet toxicity at day 2 post-treatment, followed by high platelet counts at days 5–6 post-treatment (Fig 6C
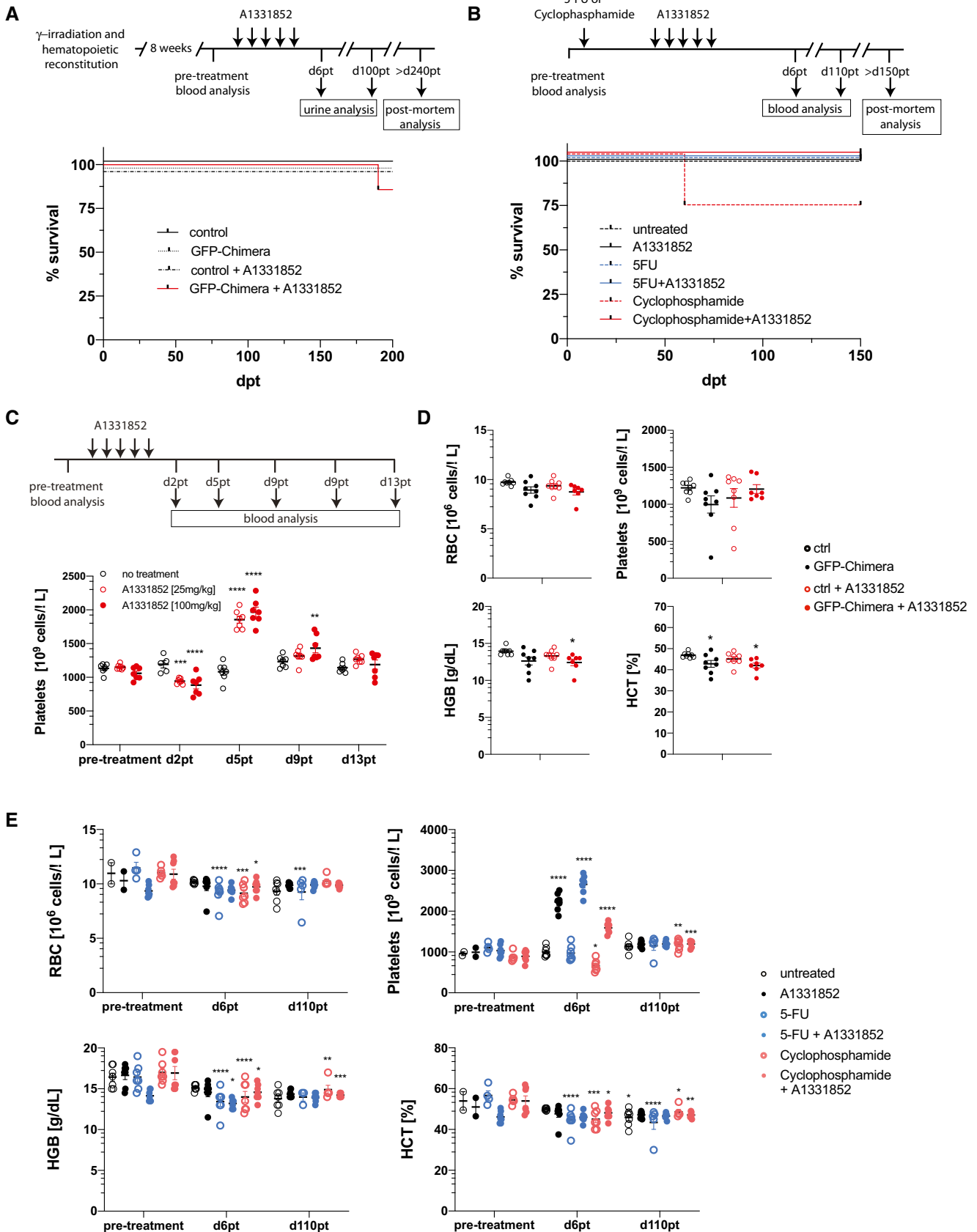
Figure 6.

and E). All mice recovered within ~ 10 days (Fig 6C). This is consistent with the described BCL-XL dependency of platelets and thus platelet toxicity followed by the rapid induction of a rebound production of platelets upon treatment with BCL-XL-inhibiting BH3 mimetic drugs (Mason *et al*, 2007; Wilson *et al*, 2010; Leverson *et al*, 2015; Merino *et al*, 2018). As reported (Brinkmann *et al*, 2017), treatment with 5-FU caused mild anemia (Fig 6E), and mice that were treated with cyclophosphamide showed a reduction in lymphocytes at day 6 post-treatment (Appendix Fig S6D). Importantly, for all drug-treated mice, the numbers of RBCs, platelets, as well as HGB and HCT values, and WBC counts were all in the normal range at the termination of the experiment (Fig 6D and E, and Appendix Fig S6B and D).

The *GFP-Chimeras* were slightly lighter and had smaller kidneys and spleens at the end of the experiment (Fig 7A and Appendix Fig S6A). However, urine testing (at 10 and 100 days post-treatment) did not provide evidence of kidney damage. No significant differences in the weights of the kidneys or spleens were observed between mice that were treated with 5-FU or cyclophosphamide alone, or in combination with A1331852, when compared to untreated mice (Fig 7B). Histological analysis revealed normal architecture of the kidneys (Fig 7C and D), liver, spleen, and bone marrow in all experimental and control mice (Appendix Fig S7).

These results show that the combination of DNA damage-inducing anti-cancer therapy plus a BCL-XL inhibitor can be tolerated, at least when administered sequentially.

Discussion

TBI and DNA damage-inducing drugs are current mainstays of cancer therapy. Apart from inducing the death of malignant cells, these treatments can also cause damage to diverse healthy tissues, including the kidney, with the underlying mechanisms still not well understood. In mice that received TBI prior to bone marrow transplantation, we found that genetic deletion of BCL-XL exclusively in non-hematopoietic cells resulted in secondary anemia due to kidney damage. This could be substantially delayed by the concomitant loss of pro-apoptotic PUMA or BIM. This reveals that in the context of DNA damage, BCL-XL is critical for the sustained survival of renal tubular epithelial cells in the adult. Notably, BCL-2 loss results in

severe polycystic kidney disease that starts during embryonic development (in the absence of DNA damage) (Veis *et al*, 1993; Bouillet *et al*, 2001). This indicates that BCL-2 and BCL-XL are both required to maintain renal tubule epithelial cell survival, the former during development and the latter in adulthood.

Radiation-induced nephropathy (RN) is frequently observed in cancer patients receiving TBI and bone marrow transplants (10–25%; Cohen, 2000; Cohen & Robbins, 2003; Cohen *et al*, 2010). Interestingly, only some TBI patients develop renal injury/failure, and the reasons for this are currently unknown (Cohen & Robbins, 2003). Our findings suggest that BCL-XL is essential to ensure the survival of renal cells that had previously sustained DNA damage, whereas undamaged cells can more readily tolerate the loss of BCL-XL. The reasons for this could be that undamaged cells might express higher levels of pro-survival BCL-2 family members other than BCL-XL (e.g., BCL-2, MCL-1) or that damaged cells express higher levels of pro-apoptotic BH3-only proteins (Campbell & Tait, 2018; Merino *et al*, 2018). This hypothesis is supported by our demonstration that the concomitant loss of the BH3-only proteins BIM or PUMA can markedly delay kidney damage and secondary anemia caused by the combination of TBI and inducible loss of BCL-XL. Perhaps patients susceptible to RN express higher basal levels of BH3-only proteins in renal tissues, possibly because they are subjected to certain stresses already. Alternatively, these cells may express abnormally low levels of pro-survival BCL-2 family members, possibly because they receive lower levels of growth factors (e.g., EGF, FGF).

All structures of the kidney can be affected by RN, including blood vessels, glomeruli, tubular epithelia, and the interstitium (Cohen & Robbins, 2003). Our histological analysis indicates that the primary pathology is apoptosis of the proximal renal tubular epithelium rather than endothelial or glomerular damage. Proximal renal tubular epithelium cells are particularly rich in mitochondria and subjected to stress due to their constant H^+-pumping. This might render these cells prone to the induction of apoptosis driven by DNA damage and the loss of BCL-XL. The deposits within the renal papillae are likely due to the accumulation of apoptotic debris and precipitates from concentrated urine in the loops of Henle or collecting ducts. These secondary obstructive changes are likely to have caused the chronic renal failure (consistent with the observed polyuria) and the segmental cortical scarring and glomerular

---

Figure 7. Pharmacological inhibition of BCL-XL in combination with DNA damage-inducing chemotherapeutics or γ-radiation at clinically relevant doses does not impair kidney function and architecture.

A GFP-Chimeras were treated with the BCL-XL inhibitor A1331852 (*n* = 8, 5 doses by oral gavage, 25 mg/kg body weight each dose). Control groups (*n* = 8 each group) include untreated GFP-Chimera and unirradiated C57BL/6-Ly5.1 (wild-type) mice treated with the BCL-XL inhibitor A1331852 or left untreated. Kidney (left panel) and spleen weights (right panel) were measured in drug-treated GFP-Chimeras or control mice at the termination of the experiment (*n* = 8 each group). Data are presented as mean ± SEM. Each data point represents one individual mouse. Statistical significance was assessed using one-way ANOVA analysis with Tukey's multiple comparisons test. No statistically significant differences were observed.

B C57BL/6-Ly5.1 (wild-type) mice (females, aged 10 weeks) were treated with cyclophosphamide (*n* = 7, 150 mg/kg body weight, 1 dose *i.v.*) or 5-fluorouracil (5-FU, *n* = 7, 100 mg/kg body weight, 1 dose *i.v.*) and after 5 days additionally treated with the BCL-XL inhibitor A1331852 (5 doses by oral gavage, 100 mg/kg body weight each dose). Control groups (*n* = 7 each group) include C57BL/6-Ly5.1 (wild-type) mice (females, aged 10 weeks) treated with the BCL-XL inhibitor A1331852 alone, cyclophosphamide alone, 5-FU alone, or left untreated. Kidney (left panel) and spleen weights (right panel) were measured in drug-treated mice or control mice at the termination of the experiment (*n* = 7 each group). Data are presented as mean ± SEM. Each data point represents one individual mouse. Statistical significance was assessed using one-way ANOVA analysis with Tukey's multiple comparisons test. No statistically significant differences were observed.

C Histological analysis of H&E-stained sections of the kidneys of drug-treated GFP-Chimeras or control mice at the termination of the experiment. Pictures are representative of at least 3 mice for each treatment group.

D Histological analysis of H&E-stained sections of the kidneys of drug-treated mice or control untreated mice at the termination of the experiment. Pictures are representative of at least 3 mice for each treatment group.
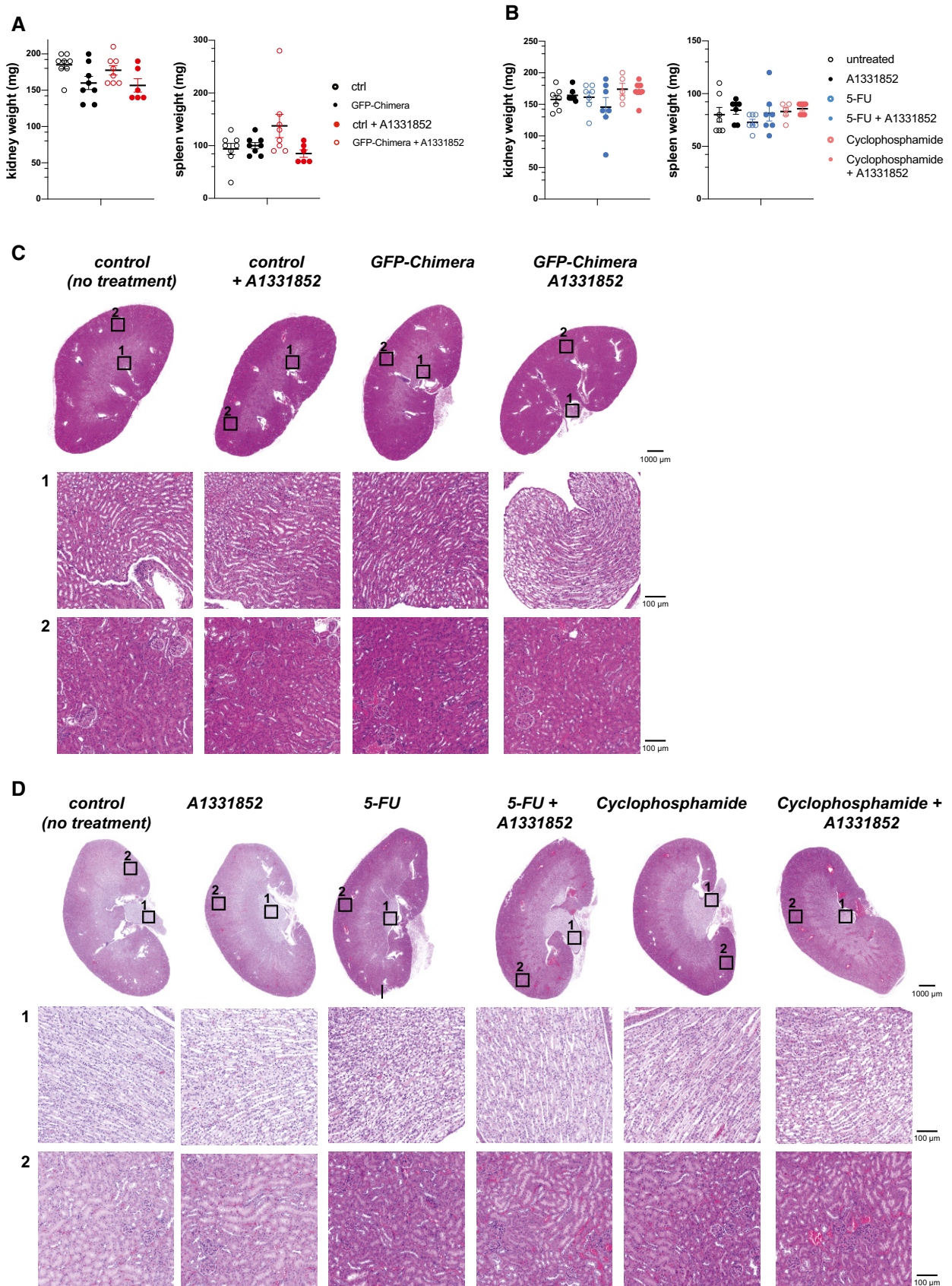
Figure 7.

changes (consistent with proteinuria). The glomerular changes are most likely a secondary effect and not directly caused by TBI as they were not seen in the control *RosaCreERT2*$^{+/Ki}$;*GFP-Chimeras*.

Besides TBI, genotoxic (e.g., cisplatin, cytarabine) and non-genotoxic drugs (e.g., cyclosporine, methotrexate) can induce kidney damage. With the advent of BH3-mimetic drugs for cancer therapy (Merino *et al*, 2018), it is important to understand what toxicities might arise from their combination with TBI or standard chemotherapeutics. We found that combinations of the BCL-XL-specific BH3-mimetic A1331852 with TBI, 5-FU, or cyclophosphamide were tolerable in mice, at least when administered sequentially. Importantly, none of the treated mice presented with thrombocytopenia 10 days after drug treatment even though, as expected (Leverson *et al*, 2015), treatment with A1331852 caused an initial reduction in platelets. This reveals that genetic irreversible loss of *Bcl-x* has more severe consequences than pharmacological inhibition of BCL-XL for a defined period. This conclusion is reminiscent of the findings from investigations comparing the impact of genetic loss of pro-survival MCL-1 vs. treatment of mice for a defined period with an MCL-1-specific BH3-mimetic drug (Kotschy *et al*, 2016; Caenepeel *et al*, 2018). These and other studies (Brinkmann *et al*, 2017; Brennan *et al*, 2018) suggest that it may be possible to establish therapeutic windows for combination treatment using BH3-mimetic drugs and standard chemotherapy or radiation.

Materials and Methods

Mice

Bc-lx$^{fl/fl}$ (Wagner *et al*, 2000), *Bim*$^{-/-}$ (Bouillet *et al*, 1999b), *Puma*$^{-/-}$ (Villunger *et al*, 2003), UBC-GFP Tg (Schaefer *et al*, 2001), and *RosaCreERT2* mice (Seibler *et al*, 2003) have been described. All mice were either generated on a C57BL/6 background or had been backcrossed onto this background for at least 20 generations. All experiments with mice were conducted according to the guidelines of The Walter and Eliza Hall Institute of Medical Research Animal Ethics Committee.

Generation of bone marrow chimeras

Recipient mice were subjected to two doses of 5.5 Gy γ-irradiation given 3 h apart. After 2 h, mice were transplanted with $3–6 \times 10^6$ UBC-GFP Tg bone marrow cells. Successful hematopoietic reconstitution was verified by detecting GFP$^+$ blood cells by FACS.

Chemotherapeutic drug treatment

To activate CreERT2, mice were given 200 mg/kg body weight tamoxifen (Sigma-Aldrich) in peanut oil/10% ethanol daily over 3 days by oral gavage 8 weeks post-transplantation. The BCL-XL inhibitor A1331852 was synthesized in house, dissolved in 60% Phosal PG 50, 27.5% polyethylene glycol 400 (PEG-400), 10% ethanol, and 2.5% DMSO, and administered by oral gavage. Working solutions of 5-fluorouracil and cyclophosphamide (Sigma-Aldrich) were prepared according to the manufacturer's instructions, and a maximum volume of 200 µl was injected into the tail vein (*i.v.*) of mice.

Isolation of renal proximal tubule cells

For each adult mouse, both kidneys were finely minced and dissociated in 2 ml disaggregation buffer (4 mg/ml Collagenase IV (C51380-1G, Sigma), 1 mg/ml DNAseI (DN25-100 mg, Sigma), 2 mg/ml Dispase (17105-041, Gibco), and 2 mg/ml Hyaluronidase (H3506, Sigma) in PBS). The mixture was incubated at 37°C for 30 min with frequent agitation, and an equal volume of neutralization buffer (20% dialyzed fetal bovine serum (FBS) and 5 mM EDTA in PBS) was added. The sample was centrifuged at $600 \times g$ at room temperature for 8 min, and pelleted cells were resuspended in 1 ml of FACS buffer (2% dialyzed FBS and 5 mM EDTA in PBS) and passed through a 70-µm cell strainer (431751, Corning). EasySep™ Mouse Biotin Positive Selection Kit (17665, Stem Cell Technologies) was used to isolate proximal tubule cells from the cell suspension according to the manufacturer's protocol (5 µl LTL-biotin (B-1325, Vector Laboratories), 5 µl Mouse FcR Blocker, 100 µl EasySep™ Biotin Selection Cocktail, and 80 µl EasySep™ Dextran RapidSpheres™ for each sample). $2–6 \times 10^6$ cells were typically obtained for each kidney sample. 500 µl of PBS was added to the isolated proximal tubule cells and resuspended (which equated to a total volume of ~ 600 µl). 100 µl of cells was aliquoted into 200 µl of 0.25% NP40 Tris lysis buffer (1× TBS with Roche complete mini protease and PhosSTOP inhibitor tablets), TRIzol or eBioscience Fixative, each prepared in duplicate. A sample of isolated cells was grown on 8-well chamber slides (80826, IBIDI) and coated with 2 µg/cm^2 collagen IV (5022, Advanced Biomatrix) overnight at 37°C. 300 µl of fixative solution (4% paraformaldehyde, 0.1% Triton X-100 in DPBS) was added to isolated proximal tubule cells grown overnight in 8-well chamber slides and incubated for 10 min at room temperature. 300 µl of blocking solution (1% BSA in PBS) was added and incubated for 10 min at room temperature. Primary label, LTL-Biotin (1:250 dilution) in blocking solution, was added to the cells and incubated at room temperature for 2 h followed by secondary antibodies in blocking solution labeled with Streptavidin-Alexa Fluor 488, and 4′,6-diamidino-2-phenylindole (DAPI, to stain DNA) was added and samples incubated for 1.5 h at room temperature. 100 µl of Fluoromount G mounting medium (0100-01, Southern Biotech) was added to each well, and images were acquired using a Leica SP8 confocal microscope at the Monash Micro Imaging (MMI) facility.

RNA extraction and quantitative RT–PCR

RNA was extracted using the standard phenol-chloroform extraction protocol using TRIzol™ (Ambion Inc). Isolated RNA was reverse-transcribed using oligo-dT primers and the Superscript III First Strand cDNA Synthesis Kit (Invitrogen) according to the manufacturer's instructions. Quantitative RT–PCR reactions were performed in triplicate using the TaqMan™ Fast Advanced Master Mix (Applied Biosystems) for *Bax* (Cat#Mm00432050_m1), *Bak* (Cat#Mm00432045_m1), *Bbc3* (*Puma*, Cat#Mm00519268_m1), *Pmaip1* (*Noxa*, Cat#Mm00451763_m1), *Bcl2l11* (Bim, Cat#Mm00437796_m1), *Bcl2* (Cat#Mm00477631_m1), *Bcl2A1* (Cat#Mm03646861), *Bcl2l1* (*Bcl-x*, Cat#Mm00437783), and *Mcl1* (Cat#Mm01257351_g1). Data were collected using the Viia7 PCR System (Thermo Fischer Scientific) using the Viia7™ software package (Thermo Fischer Scientific).

Probing for *GapDH* (Cat#Mm99999915_g1) served as a house-keeping gene. Data were calculated using the $2^{-\Delta\Delta Ct}$ method.

Western blot analysis

Cells were lysed using 0.25% NP40 Tris lysis buffer (1× TBS with Roche complete mini protease and PhosSTOP inhibitor tablets). Western Blot analysis was performed using specific antibodies detecting MCL-1 (clone 14C11-20, gift from D.C.S Huang), BCL-XL (polyclonal, Becton Dickinson), BCL-2 (clone 7/Bcl-2, Becton Dickinson), BIM (polyclonal, Enzo), BAK (clone 4B5 (Dewson *et al*, 2008)), and BAX (clone 49F9, gift from D.C.S Huang).

Serum analysis

Sera were stored at −20°C and analyzed using Architect c1600 (Abbott Diagnostics,).

Histology

Tissues were harvested and fixed in 10% formalin. Sections (75 μm) were stained with hematoxylin and eosin (H&E) and examined by an experimenter who was blinded to the genotype and treatment of the mice.

TUNEL staining

TUNEL staining was performed as described (Ke *et al*, 2018). Slides were scored by microscopy in a blinded manner. Kidney sections were divided into ~ 40 microscopic images, and the percentage of blue (TUNEL$^+$) vs. brown nuclei was determined using a personalized script for ImageJ. Data points shown represent average values for each kidney section.

Microscopy

For multi-photon microscopy, kidneys were fixed in 4% paraformaldehyde overnight at 4°C and embedded in 3% low-melting point agarose (Sigma- Aldrich). Sections (500 μM) were mounted on slides in glycerol. Images were acquired on an Olympus FVMPE-RS Multiphoton system equipped with a Mai-Tai eHP DeepSee multi-photon laser and processed using CellSens software (Olympus).

For confocal imaging, kidneys were fixed in 10% formalin. Sections (75 μm) were mounted on adherent microscopic slides (Sarstedt). Slides were blocked in 2% normal donkey serum and 1% Triton X-100 in PBS for 20 min at RT and stained overnight with rat-anti-PECAM1/CD31 antibodies (1/100, clone Mec13.3, BD PharMingen) in blocking solution and secondary Alexa594 goat anti-rat IgG antibodies and DAPI (Invitrogen) in blocking solution for 1 h. Slides were imaged using a Zeiss LSM780.

Statistical analysis

Data were plotted and analyzed with Prism (GraphPad Software Inc). Statistical comparisons were conducted using unpaired two-tailed Student's *t*-test assuming equal variance or one-way ANOVA analysis with Tukey's multiple comparisons test. The number of replicates for each experiment is indicated in the respective figure legends. No mice were excluded for statistical analysis.

Data availability

No primary data sets are associated with this study.

Expanded View for this article is available online.

Authorship contributions

KB, SGr, SGl, and AS designed the study. MJH helped with the design of experiments. KB conducted all experiments. PW performed pathological analysis of tissue specimens. ARDD and GLK helped with some experiments. VW helped with the multi-photon microscopic analysis. LW performed the quantification of the TUNEL assays. DLC, MST, and IMS helped with the purification of proximal tubular epithelial cells. DN and GL provided the BCL-XL inhibitor A1331852 and provided advice for the use of this drug. KB, PW, and AS wrote the manuscript and all other authors edited it.

Conflict of interest

The authors declare that they have no conflict of interest.

References

Adams JM, Cory S (2007) The Bcl-2 apoptotic switch in cancer development and therapy. *Oncogene* 26: 1324−1337

Adams JM, Cory S (2018) The BCL-2 arbiters of apoptosis and their growing role as cancer targets. *Cell Death Differ* 25: 27−36

Arbour N, Vanderluit JL, Le Grand JN, Jahani-Asl A, Ruzhynsky VA, Cheung EC, Kelly MA, MacKenzie AE, Park DS, Opferman JT *et al* (2008) Mcl-1 is a key regulator of apoptosis during CNS development and after DNA damage. *J Neurosci* 28: 6068−6078

Beroukhim R, Mermel CH, Porter D, Wei G, Raychaudhuri S, Donovan J, Barretina J, Boehm JS, Dobson J, Urashima M *et al* (2010) The landscape of somatic copy-number alteration across human cancers. *Nature* 463: 899−905

Bouillet P, Cory S, Zhang LC, Strasser A, Adams JM (2001) Degenerative disorders caused by Bcl-2 deficiency prevented by loss of its BH3-only antagonist Bim. Dev Cell 1: 645−653

Bouillet P, Metcalf D, Huang DC, Tarlinton DM, Kay TW, Kontgen F, Adams JM, Strasser A (1999a) Proapoptotic Bcl-2 relative Bim required for certain apoptotic responses, leukocyte homeostasis, and to preclude autoimmunity. Science 286: 1735−1738

Bouillet P, Metcalf D, Huang DCS, Tarlinton DM, Kay TWH, Köntgen F, Adams JM, Strasser A (1999b) Proapoptotic Bcl-2 relative Bim required for certain apoptotic responses, leukocyte homeostasis, and to preclude autoimmunity. Science 286: 1735−1738

Brennan MS, Chang C, Tai L, Lessene G, Strasser A, Dewson G, Kelly GL, Herold MJ (2018) Humanized Mcl-1 mice enable accurate preclinical evaluation of MCL-1 inhibitors destined for clinical use. Blood 132: 1573−1583

Brinkmann K, Grabow S, Hyland CD, Teh CE, Alexander WS, Herold MJ, Strasser A (2017) The combination of reduced MCL-1 and standard chemotherapeutics is tolerable in mice. Cell Death Differ 24: 2032−2043

Caenepeel S, Brown SP, Belmontes B, Moody G, Keegan KS, Chui D, Whittington DA, Huang X, Poppe L, Cheng AC et al (2018) AMG 176, a selective MCL1 inhibitor, is effective in hematologic cancer models alone and in combination with established therapies. Cancer Discov 8: 1582−1597

Campbell KJ, Tait SWG (2018) Targeting BCL-2 regulated apoptosis in cancer. Open Biol 8: 180002

Cohen EP (2000) Radiation nephropathy after bone marrow transplantation. Kidney Int 58: 903−918

Cohen EP, Robbins ME (2003) Radiation nephropathy. Semin Nephrol 23: 486−499

Cohen EP, Pais P, Moulder JE (2010) Chronic kidney disease after hematopoietic stem cell transplantation. Semin Nephrol 30: 627−634

Cragg MS, Kuroda J, Puthalakath H, Huang DC, Strasser A (2007) Gefitinib-induced killing of NSCLC cell lines expressing mutant EGFR requires BIM and can be enhanced by BH3 mimetics. PLoS Med 4: 1681−1689. discussion 1690

Cragg MS, Jansen ES, Cook M, Harris C, Strasser A, Scott CL (2008) Treatment of B-RAF mutant human tumor cells with a MEK inhibitor requires Bim and is enhanced by a BH3 mimetic. J Clin Invest 118: 3651−3659

Davis SL, Littlewood TJ (2012) The investigation and treatment of secondary anaemia. Blood Rev 26: 65−71

Del Gaizo MV, Letai A (2013) BH3 profiling−measuring integrated function of the mitochondrial apoptotic pathway to predict cell fate decisions. Cancer Lett 332: 202−205

Dewson G, Kratina T, Sim HW, Puthalakath H, Adams JM, Colman PM, Kluck RM (2008) To trigger apoptosis, Bak exposes its BH3 domain and homodimerizes via BH3:groove interactions. Mol Cell 30: 369−380

Dracham CB, Shankar A, Madan R (2018) Radiation induced secondary malignancies: a review article. Radiat Oncol J 36: 85−94

Erlacher M, Michalak EM, Kelly PN, Labi V, Niederegger H, Coultas L, Adams JM, Strasser A, Villunger A (2005) BH3-only proteins Puma and Bim are rate-limiting for gamma-radiation- and glucocorticoid-induced apoptosis of lymphoid cells in vivo. Blood 106: 4131−4138

Francois A, Milliat F, Guipaud O, Benderitter M (2013) Inflammation and immunity in radiation damage to the gut mucosa. Biomed Res Int 2013: 123241

Gavrieli Y, Sherman Y, Ben-Sasson SA (1992) Identification of programmed cell death in situ via specific labeling of nuclear DNA fragmentation. J Cell Biol 119: 493−501

Glaser SP, Lee EF, Trounson E, Bouillet P, Wei A, Fairlie WD, Izon DJ, Zuber J, Rappaport AR, Herold MJ et al (2012) Anti-apoptotic Mcl-1 is essential for

the development and sustained growth of acute myeloid leukemia. Genes Dev 26: 120−125

Gorczyca W, Bruno S, Darzynkiewicz R, Gong J, Darzynkiewicz Z (1992) DNA strand breaks occurring during apoptosis - their early insitu detection by the terminal deoxynucleotidyl transferase and nick translation assays and prevention by serine protease inhibitors. Int J Oncol 1: 639−648

Hanahan D, Weinberg RA (2000) The hallmarks of cancer. Cell 100: 57−70

Hanahan D, Weinberg RA (2011) Hallmarks of cancer: the next generation. Cell 144: 646−674

Ke FFS, Vanyai HK, Cowan AD, Delbridge ARD, Whitehead L, Grabow S, Czabotar PE, Voss AK, Strasser A (2018) Embryogenesis and adult life in the absence of intrinsic apoptosis effectors BAX, BAK, and BOK. Cell 173: 1217−1230 e1217

Kelly GL, Grabow S, Glaser SP, Fitzsimmons L, Aubrey BJ, Okamoto T, Valente LJ, Robati M, Tai L, Fairlie WD et al (2014) Targeting of MCL-1 kills MYC-driven mouse and human lymphomas even when they bear mutations in p53. Genes Dev 28: 58−70

Khan S, Zhang X, Lv D, Zhang Q, He Y, Zhang P, Liu X, Thummuri D, Yuan Y, Wiegand JS et al (2019) A selective BCL-XL PROTAC degrader achieves safe and potent antitumor activity. Nat Med 25: 1938−1947

Kim J, Jung Y (2017) Radiation-induced liver disease: current understanding and future perspectives. Exp Mol Med 49: e359

Kotschy A, Szlavik Z, Murray J, Davidson J, Maragno AL, Le Toumelin-Braizat G, Chanrion M, Kelly GL, Gong JN, Moujalled DM et al (2016) The MCL1 inhibitor S63845 is tolerable and effective in diverse cancer models. Nature 538: 477−482

Wang L, Doherty GA, Judd AS, Zhi-Fu T, Hansen M, Frey RR, Xiaohong Song ARK, Wang X, Wendt MD, Flygare JA et al (2020) Discovery of A-1331852, a first-in-class, potent and orally-bioavailable BCL-XL inhibitor. ACS Med Chem Lett 11: 1829−1836

Lessene G, Czabotar PE, Sleebs BE, Zobel K, Lowes KN, Adams JM, Baell JB, Colman PM, Deshayes K, Fairbrother WJ et al (2013) Structure-guided design of a selective BCL-X(L) inhibitor. Nat Chem Biol 9: 390−397

Leverson JD, Phillips DC, Mitten MJ, Boghaert ER, Diaz D, Tahir SK, Belmont LD, Nimmer P, Xiao Y, Ma XM et al (2015) Exploiting selective BCL-2 family inhibitors to dissect cell survival dependencies and define improved strategies for cancer therapy. Sci Transl Med 7: 279ra240

Marks LB, Yu X, Vujaskovic Z, Small Jr W, Folz R, Anscher MS (2003) Radiation-induced lung injury. Semin Radiat Oncol 13: 333−345

Mason KD, Carpinelli MR, Fletcher JI, Collinge JE, Hilton AA, Ellis S, Kelly PN, Ekert PG, Metcalf D, Roberts AW et al (2007) Programmed anuclear cell death delimits platelet life span. Cell 128: 1173−1186

Mehta V (2005) Radiation pneumonitis and pulmonary fibrosis in non-small-cell lung cancer: pulmonary function, prediction, and prevention. Int J Radiat Oncol Biol Phys 63: 5−24

Merino D, Kelly GL, Lessene G, Wei AH, Roberts AW, Strasser A (2018) BH3-mimetic drugs: blazing the trail for new cancer medicines. Cancer Cell 34: 879−891

Motoyama N, Wang F, Roth KA, Sawa H, Nakayama K, Nakayama K, Negishi I, Senju S, Zhang Q, Fujii S et al (1995) Massive cell death of immature hematopoietic cells and neurons in Bcl-x-deficient mice. Science 267: 1506−1510

Ogilvy-Stuart AL, Shalet SM (1993) Effect of radiation on the human reproductive system. Environ Health Perspect 101(Suppl 2): 109−116

Olcina MM, Giaccia AJ (2016) Reducing radiation-induced gastrointestinal toxicity − the role of the PHD/HIF axis. J Clin Invest 126: 3708−3715

Oltersdorf T, Elmore SW, Shoemaker AR, Armstrong RC, Augeri DJ, Belli BA, Bruncko M, Deckwerth TL, Dinges J, Hajduk PJ et al (2005) An inhibitor of

Bcl-2 family proteins induces regression of solid tumours. *Nature* 435: 677−681

Opferman JT, Iwasaki H, Ong CC, Suh H, Mizuno S, Akashi K, Korsmeyer SJ (2005) Obligate role of anti-apoptotic MCL-1 in the survival of hematopoietic stem cells. *Science* 307: 1101−1104

Print CG, Loveland KL, Gibson L, Meehan T, Stylianou A, Wreford N, de Kretser D, Metcalf D, Kontgen F, Adams JM *et al* (1998) Apoptosis regulator bcl-w is essential for spermatogenesis but appears otherwise redundant. *Proc Natl Acad Sci USA* 95: 12424−12431

Riedl SJ, Salvesen GS (2007) The apoptosome: signalling platform of cell death. *Nat Rev Mol Cell Biol* 8: 405−413

Rinkenberger JL, Horning S, Klocke B, Roth K, Korsmeyer SJ (2000) Mcl-1 deficiency results in peri-implantation embryonic lethality. *Genes Dev* 14: 23−27

Rucker 3rd EB, Dierisseau P, Wagner KU, Garrett L, Wynshaw-Boris A, Flaws JA, Hennighausen L (2000) Bcl-x and Bax regulate mouse primordial germ cell survival and apoptosis during embryogenesis. *Mol Endocrinol* 14: 1038−1052

Schaefer BC, Schaefer ML, Kappler JW, Marrack P, Kedl RM (2001) Observation of antigen-dependent CD8^{+} T-cell/ dendritic cell interactions *in vivo*. *Cell Immunol* 214: 110−122

Schenk RL, Tuzlak S, Carrington EM, Zhan Y, Heinzel S, Teh CE, Gray DH, Tai L, Lew AM, Villunger A *et al* (2017) Characterisation of mice lacking all functional isoforms of the pro-survival BCL-2 family member A1 reveals minor defects in the haematopoietic compartment. *Cell Death Differ* 24: 534−545

Seibler J, Zevnik B, Kuter-Luks B, Andreas S, Kern H, Hennek T, Rode A, Heimann C, Faust N, Kauselmann G *et al* (2003) Rapid generation of inducible mouse mutants. *Nucleic Acids Res* 31: e12

Souers AJ, Leverson JD, Boghaert ER, Ackler SL, Catron ND, Chen J, Dayton BD, Ding H, Enschede SH, Fairbrother WJ *et al* (2013) ABT-199, a potent and selective BCL-2 inhibitor, achieves antitumor activity while sparing platelets. *Nat Med* 19: 202−208

Tait SW, Green DR (2010) Mitochondria and cell death: outer membrane permeabilization and beyond. *Nat Rev Mol Cell Biol* 11: 621−632

Thomas RL, Roberts DJ, Kubli DA, Lee Y, Quinsay MN, Owens JB, Fischer KM, Sussman MA, Miyamoto S, Gustafsson AB (2013) Loss of MCL-1 leads to impaired autophagy and rapid development of heart failure. *Genes Dev* 27: 1365−1377

Tse C, Shoemaker AR, Adickes J, Anderson MG, Chen J, Jin S, Johnson EF, Marsh KC, Mitten MJ, Nimmer P *et al* (2008) ABT-263: a potent and orally bioavailable Bcl-2 family inhibitor. *Can Res* 68: 3421−3428

Tuzlak S, Schenk RL, Vasanthakumar A, Preston SP, Haschka MD, Zotos D, Kallies A, Strasser A, Villunger A, Herold MJ (2017) The BCL-2 pro-survival protein A1 is dispensable for T cell homeostasis on viral infection. *Cell Death Differ* 24: 523−533

Uhlen M, Bjorling E, Agaton C, Szigyarto CA, Amini B, Andersen E, Andersson AC, Angelidou P, Asplund A, Asplund C *et al* (2005) A human protein atlas for normal and cancer tissues based on antibody proteomics. *Mol Cell Proteomics* 4: 1920−1932

Uhlen M, Zhang C, Lee S, Sjostedt E, Fagerberg L, Bidkhori G, Benfeitas R, Arif M, Liu Z, Edfors F *et al* (2017) A pathology atlas of the human cancer transcriptome. *Science* 357: eaan2507

Veis DJ, Sorenson CM, Shutter JR, Korsmeyer SJ (1993) Bcl-2-deficient mice demonstrate fulminant lymphoid apoptosis, polycystic kidneys, and hypopigmented hair. *Cell* 75: 229−240

Villunger A, Michalak EM, Coultas L, Mullauer F, Bock G, Ausserlechner MJ, Adams JM, Strasser A (2003) p53- and drug-induced apoptotic responses mediated by BH3-only proteins puma and noxa. *Science* 302: 1036−1038

Vooijs M, Jonkers J, Berns A (2001) A highly efficient ligand-regulated Cre recombinase mouse line shows that LoxP recombination is position dependent. *EMBO Rep* 2: 292−297

Wagner KU, Claudio E, Rucker 3rd EB, Riedlinger G, Broussard C, Schwartzberg PL, Siebenlist U, Hennighausen L (2000) Conditional deletion of the Bcl-x gene from erythroid cells results in hemolytic anemia and profound splenomegaly. *Development* 127: 4949−4958

Wang X, Bathina M, Lynch J, Koss B, Calabrese C, Frase S, Schuetz JD, Rehg JE, Opferman JT (2013) Deletion of MCL-1 causes lethal cardiac failure and mitochondrial dysfunction. *Genes Dev* 27: 1351−1364

Weiss G, Goodnough LT (2005) Anemia of chronic disease. *N Engl J Med* 352: 1011−1023

Wilson WH, O'Connor OA, Czuczman MS, LaCasce AS, Gerecitano JF, Leonard JP, Tulpule A, Dunleavy K, Xiong H, Chiu YL *et al* (2010) Navitoclax, a targeted high-affinity inhibitor of BCL-2, in lymphoid malignancies: a phase 1 dose-escalation study of safety, pharmacokinetics, pharmacodynamics, and antitumour activity. *Lancet Oncol* 11: 1149−1159